

RESEARCH ARTICLE

10.1029/2018JB017157

Key Points:

- Electrical resistivity of FeP, Fe₂P, and Fe₃P was measured at pressures of 1.3–3.2 GPa and temperatures up to 1800 K using four-wire methods
- Phosphorus has higher impurity resistivity than silicon at high-pressure and high-temperature conditions
- Electrical resistivity drop of Fe₃P upon melting may yield a discontinuity on the thermal state at solid inner and liquid outer cores

Supporting Information:

- Supporting Information S1

Correspondence to:

S. Zhai,
zhaishuangmeng@mail.gyig.ac.cn

Citation:

Yin, Y., Zhai, K., Zhang, B., & Zhai, S. (2019). Electrical resistivity of iron phosphides at high-pressure and high-temperature conditions with implications for lunar core's thermal conductivity. *Journal of Geophysical Research: Solid Earth*, 124, 5544–5556. <https://doi.org/10.1029/2018JB017157>


Received 11 DEC 2018

Accepted 21 MAY 2019

Accepted article online 29 MAY 2019

Published online 21 JUN 2019

Electrical Resistivity of Iron Phosphides at High-Pressure and High-Temperature Conditions With Implications for Lunar Core's Thermal Conductivity

Yuan Yin^{1,2}, Kuan Zhai^{1,2}, Baohua Zhang¹ , and Shuangmeng Zhai¹ 

¹Key Laboratory of High-Temperature and High-Pressure Study of the Earth's Interior, Institute of Geochemistry, Chinese Academy of Sciences, Guiyang, China, ²University of Chinese Academy of Sciences, Beijing, China

Abstract Based on cosmochemistry evidence and element partitioning experiments, phosphorus is thought to be present in the iron-rich cores of Earth and Moon. Phosphorus has a similar effect as silicon and sulfur on the electrical and thermal transport properties of iron at core conditions. However, the magnitude of the impurity scattering caused by phosphorus, the temperature dependence of iron phosphorus compounds, and the change across melting all have not been intensively investigated. We measured the electrical resistivity of Fe₃P, Fe₂P, and FeP using a four-wire method at 1.3 to 3.2 GPa and temperatures up to 1800 K. We also identify the melting temperatures of FeP, Fe₂P, and Fe₃P by sudden changes in resistivity upon heating. The present experimental results demonstrate that phosphorus can enhance the electrical resistivity of iron more effectively than silicon. The resistivity of iron phosphides decreases with increasing pressures and decreasing phosphorus content. The resistivity of Fe-P alloys obeys the Matthiessen's rule, which describes the positive linear correlation between resistivity and phosphorus content. This finding is comparable to previously observed atomic order-disorder in Fe-Si and Fe-C systems. Furthermore, the resistivity of liquid Fe₂P and Fe₃P shows a negative linear correlation with temperatures. Different from pure iron, the calculated thermal conductivity of Fe₃P increases by 33% upon melting. It is speculated that the thermal conductivity of the lunar solid inner core may be much lower than that of the liquid outer core when ordered iron light element compounds (e.g., Fe₃C and Fe₃P) are present in the solid core.

1. Introduction

Addition of light elements, such as Si, S, C, and O, can dramatically increase the electrical resistivity of iron. Therefore, they must be accounted for in estimating the thermal conductivity of iron-rich planetary cores (de Koker et al., 2012; Konôpková et al., 2016; Ohta et al., 2016; Pozzo et al., 2012, 2013). Electrical resistivity measurements on solid Fe, Fe-Ni, and Fe-Si alloys at high-pressure and room temperature environment revealed that different types and content of alloy elements have different magnitude influence on the resistivity of Fe-L alloys (L, light elements; Gomi et al., 2013, 2016; Gomi & Hirose, 2015; Seagle et al., 2013). Recently, Suehiro et al. (2017) suggested that sulfur has a weaker influence than silicon by measuring the electrical resistivity of Fe-S-Si alloy (3 wt% S and 3 wt% Si) at pressures up to 110 GPa at 300 K. Zhang et al. (2018) reported the electrical resistivity of Fe₉₉C₁ alloy (1 at.% C) and iron carbides (Fe₃C, Fe₇C₃) at pressures up to 80 GPa and at 300 K, demonstrating that carbon has a stronger effect than Si, S, and Ni in reducing the electrical and thermal conductivity of the Earth's core. Despite the studies on solid phase, high-temperature and high-pressure experiments (Pommier, 2018; Silber et al., 2018) and first principles calculations (Wagle et al., 2018; Wagle & Steinle-Neumann, 2018) are all used for the resistivity of liquid Fe and liquid Fe-S system also provides precious constraints on the thermal conductivity of liquid cores.

Owing to its siderophile character and depletion in the mantle compared with CI chondrites, phosphorus is thought to be mainly stored in the Earth's core as a potential candidate light element (Newsom, 1990, 1995; Newsom & Drake, 1983; Newsom & Taylor, 1989; Righter, 2003). Partition coefficient experiments also confirmed that phosphorus preferred the metallic core in the terrestrial planets (Newsom & Drake, 1983; Righter, 2002; Righter et al., 1997, 2010; Righter & Chabot, 2011; Steenstra et al., 2016; Wood et al., 2006). According to cosmochemistry studies, phosphorus content in the core of the Earth, Mars, and Moon are estimated as 0.2 wt% (McDonough, 2003; McDonough & Sun, 1995), 0.3 wt% (Sha, 2000), and 0.1 wt% (Drake, 1987), respectively. Iron-nickel phosphide minerals, such as allabogdanite-(Fe, Ni)P,

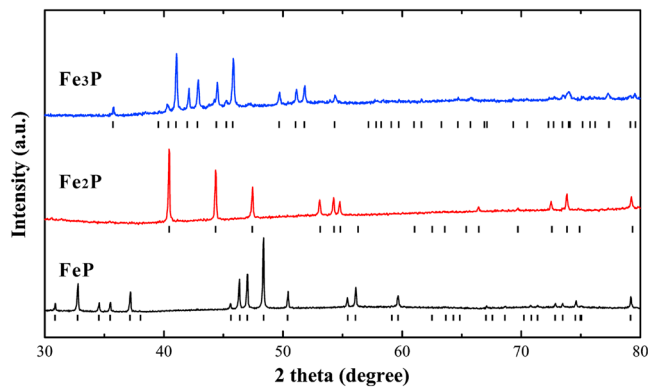


Figure 1. X-ray diffraction patterns for the synthesized iron phosphide phases. Vertical bars represent peak positions for standard iron-phosphide (PDF-# 89-2746 for FeP, PDF-# 89-3680 for Fe₂P, and PDF-# 89-2712 for Fe₃P from ICSD patterns databases).

nickelphosphide-(Ni, Fe)₂P, schreibersite-(Fe, Ni)₃P, and mellinite-(Fe, Ni)₄P are common phosphorus-bearing minerals in the iron meteorites (Britvin et al., 2002, 2015; Pratesi, 2006), which suggests phosphorus may alloy with iron in the terrestrial planet cores. Structural properties of three Fe-P compounds (iron phosphides, FeP-35.68 wt% P, Fe₂P-21.71 wt% P, and Fe₃P-15.60 wt% P) at high-pressure and high-temperature conditions have been done by experimental and theoretical methods. Like other well-investigated Fe-L system (e.g., Fe-C, Fe-S, and Fe-Si), these Fe-P compounds have similar chemical structure and crystalline structure (e.g., Fe₃C, Fe₃S, FeSi) at core pressure condition (Dera et al., 2008; Gu et al., 2011, 2014; Scott et al., 2007, 2008; Wu et al., 2011; Wu & Qin, 2010; Yan, 2015). Understanding the thermal dynamic properties and transport properties of these Fe-P compounds is essential to constrain the chemistry and physics of the metallic core of terrestrial planets.

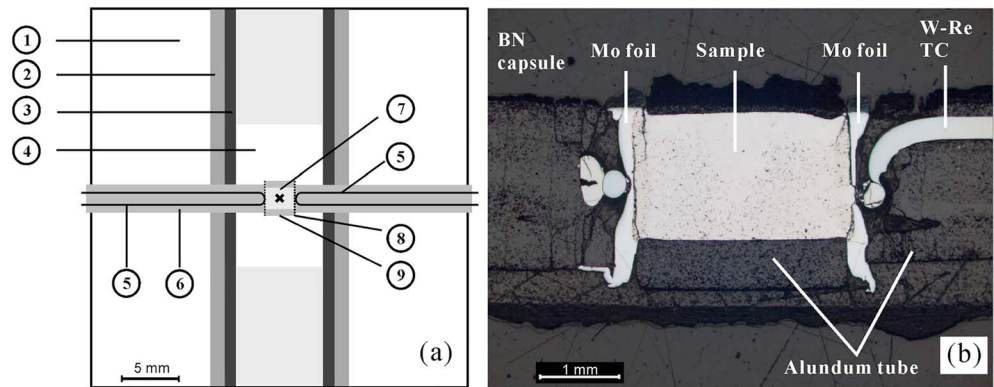
The resistivity of iron phosphides has been measured at ambient pressure in previous studies. Westerstrandh et al. (1977) reported the resistivity of the single crystal FeP to be 3 μΩ·m at 1 atm and 300 K, using the method of van der Pauw (1958). Fujii et al. (1977) measured the resistivity of single crystal Fe₂P by a standard four-probe method with a current reversal at 1 atm and up to 600 K. It is ~4.3 μΩ·m along the *b* axis and ~3 μΩ·m along the *c* axis for Fe₂P crystalline at 300 K and 1 atm. Fujiwara et al. (1980) and Abliz et al. (2006) investigated the effect of pressures on the electrical resistivity of Fe₂P up to 8 GPa at low temperatures (2.5–300 K). For Fe-P alloys, the resistivity increases linearly from 0.12 to 0.37 μΩ·m when the phosphorus content varies from 0 to 2.0 wt% at 1 atm and 300 K (Węgliński & Kaczmar, 1980). These results imply that the phosphorus can efficiently increase the resistivity of iron at ambient conditions. However, due to the absence of experiments at high-pressure and high-temperature conditions, the effect of phosphorus on the iron-rich cores in terrestrial planets has not been assessed.

In this study, we measured the electrical resistivity of three solid and liquid Fe-P compounds (FeP, Fe₂P and Fe₃P) at high-pressure and high-temperature conditions, in order to quantify the effect of phosphorus on the resistivity and thermal conductivity of iron. In addition, we estimate the thermal conductivity of solid and liquid Fe₃P at 3.2 GPa and up to 1600 K, which provide new insight on thermal conduction in the lunar solid inner core and liquid outer core.

2. Experimental Methods

2.1. Starting Materials

The samples we measured in this study are polycrystalline Fe-P compounds (FeP, Fe₂P, and Fe₃P). Sample synthesis and resistance measurement were all performed in a DS 6 × 600t cubic-anvil-type apparatus at the Institute of Geochemistry, Chinese Academy of Sciences. A series of synthetic experiments and machining processes prior to the resistance measurements were conducted in order to make a solid, well-defined shape of iron phosphides. Stoichiometric amounts of iron powder (99.99%, Alfa Aesar) and red phosphorus (99.9%, Alfa Aesar) powder were mechanically mixed and ground in ethanol in an agate mortar to synthesize FeP at 1 GPa and 1273 K for 4 hr in the same conditions as Gu et al. (2013). To ensure the quality of the synthesized iron phosphides, Fe₂P and Fe₃P were synthesized by solid state reaction at 1273 K and 1 GPa for 4 hr, using synthesized FeP and corresponding molar ratios of pure iron powder. All the aforementioned starting materials are synthesized in boron nitride capsules to avoid contamination in high-pressure assemblies. Subsequently, each of the iron phosphide powder was sealed again into the boron nitride capsules and sintered at 1 GPa and 1073 K for 5 hr, to obtain a smaller sample with suitable size. Then, the recovered samples were carefully machined into cylindrical shape with a length of ~2.5 mm and a diameter of ~1.8 mm for electrical resistivity measurement. Some of the synthesized iron phosphide powders were checked by X-ray diffractometer with Cu-Kα radiation, and the results were illustrated in Figure 1. Their refined lattice parameters are *a* = 5.186 Å, *b* = 3.097 Å, and *c* = 5.787 Å for FeP; *a* = 5.865 Å and *c* = 3.456 Å for Fe₂P; *a* = 9.100 Å and *b* = 4.462 Å for Fe₃P. These results are consistent with previous reports (Dera et al., 2008; Gu et al., 2011, 2014, Scott et al., 2007, 2008).



1: Pyrophyllite 2: Al₂O₃ sleeve 3: Graphite heater 4: Boron nitride 5: Thermocouple wires
6: Four-holes Al₂O₃ tube 7: Sample 8: Mo foil 9: Hard Al₂O₃ tube

Figure 2. The sketch (a) shows the cross section of the sample assemblages. Black cross on the sample represents a W-Re thermocouple, used to control temperatures. (b) An optical microscope image for a sectioned pressure cell (Fe₃P) recovered from 2 GPa and 1575 K. Four thermocouple wires act as current leads (cross-section view along the long axis). Black materials on the upper part of the sample in (b) are unground epoxy.

2.2. Experimental Procedures and Data Analysis

For the resistance measurement, the assembly consisted of a cubic pyrophyllite pressure medium, an Al₂O₃ sleeve, a graphite cylindrical heater, and a BN sleeve which insulates the sample from the furnace (Figure 2a). To ensure that the sample does not undergo severe deformation during the compression and melting process, a thick layer of alundum tube was used to maintain the sample geometry. On both sides of the sample, two thin molybdenum discs (a diameter of 3.0 mm and thickness of 0.2 mm) were used as electrodes to ensure good electrical contact between the sample and the geometrically imperfect thermocouple junction. Both molybdenum and tungsten discs have been used as electrodes in recent electrical resistivity measurements on Fe-S melts (Pommier, 2018) and Fe melts (Silber et al., 2018), respectively. They have ultrahigh melting temperature and are chemically inert. Before the sample melts, no chemical diffusion is measured between samples, Mo electrodes, and thermocouple. We found that the head of thermocouple can accidentally penetrate the molybdenum at high pressure. The penetration may affect the sample's geometry, but it is included in the geometry errors. The resistivity of molybdenum disc at 1 bar is assumed to be $5.52 \times 10^{-8} \Omega\cdot\text{m}$ at 300 K to $47.48 \times 10^{-8} \Omega\cdot\text{m}$ at 1800 K (Desai et al., 1984). The total resistivity contribution of the discs was estimated at $\sim 1.5\%$ for Fe₃P and less than 1% for FeP and Fe₂P at high-temperature conditions. Using the methods described by Ezenwa and Secco (2017a, 2017b) and Silber et al. (2017), four W-Re thermocouple wires (0.3-mm diameter, W5%Re–W26%Re) legs acted as electrodes during the resistance measurement, fully contacting with the molybdenum electrodes. One more thermocouple was used to monitor temperature, emplaced vertically in the center of the sample and attached to the outer of the ceramic tube. All thermocouples were threaded via four-hole alundum tubes for protection.

Samples were compressed to the desired pressure and then heated in steps of 50 K. The uncertainty in pressure is ± 0.1 GPa in this study. Pressure calibration used the melting curve of NaCl and the quartz-coesite phase transition, which are conducted at 1273–1473 K. The temperature of a sample was cycled twice to 873 K to enhance sample-electrode contact and reduce the contribution of contact resistance. To collect the accurate resistance data for solid samples at each temperature (< 1300 K), temperature was held for 3–5 min before the resistance measurement for solid specimens. During the measurement, the temperature difference between the two sides of the samples is 3–5 K at $T < 900$ K and ~ 10 K at $T < 1600$ K. We neglected the errors caused by such temperature gradient because the data collection interval is 50 K, significantly larger than typical temperature gradient.

In the electrical resistivity measurement mode, a constant 300–500 mA DC current was provided by a Keithley 2400 current SourceMeter. When the constant current passes through the same leading wires and flows through the sample, the voltage drop across the sample was collected by two other identical

W-Re wires and recorded by the Keysight 34470 digital multimeter. The sample's electrical resistance was calculated using Ohm's law:

$$R = \Delta U / I \quad (1)$$

where R is resistance, ΔU is the voltage drop, and I is the constant current. The resistivity (ρ) was later calculated from the Pouillet's law:

$$\rho = RS/L \quad (2)$$

where R , S , and L are sample resistance, sectional area, and length, respectively. At the pressures of 1.3 and 2.3 GPa, the maximum heating temperature reached to 1273 K for Fe_3P and 1573 K for FeP and Fe_2P . At 3.2 GPa, all the samples were heated over the melting temperature and the resistance was acquired rapidly. It is generally less than 30 s to collect resistance data in liquid at each temperature. It usually takes ~1 min to increase 50 K. After that, the power supply was switched off and the pressure was released slowly. To test the reliability of the present experimental measurement, the resistivity of a pure iron wire (1 mm, 99.99%, Alfa Aesar) was also measured at 1.1 GPa and up to 1473 K, using the same assemblage.

The recovered samples were mounted in epoxy and polished in a section parallel to the long axis of the cylindrical sample to obtain information of sample geometry, which is necessary for the resistivity calculation. Using the optical microscope, the diameter and length of the recovered samples were measured and shown in Figure 2b. The thermal expansion and compressibility also affect the sample's geometry, and their influence was included in the overall error calculations (2–4% for different iron phosphide due to their different resistivity level). Bulk moduli of FeP , Fe_2P , and Fe_3P used here are 250(7) (Gu et al., 2011), 165(3) (Scott et al., 2008), and 159(1) GPa (Scott et al., 2007), respectively. We used thermal expansion coefficients $1.8 \times 10^{-5}/\text{K}$ for FeP (Westerstrandh et al., 1977), $2 \times 10^{-5}/\text{K}$ for Fe_3P (Gu et al., 2014). We do not find the thermal expansion coefficient of Fe_2P and used the same value with Fe_3P as an approximation. Using P-V-T calculation, integrated contributions of pressure and temperature on the specimen volume are estimated at less than 1% during experiments.

2.3. Analytical Techniques

Microstructure was analyzed by scanning electron microscopy using a Scios electron microscope operating at a voltage of 30 kV and a current of 0.2 nA at the Institute of Geochemistry, Guiyang, China. Chemical composition of the recovered samples was analyzed using Energy Dispersive X-ray Spectrometry in Geophysical Laboratory. We found that all the recovered samples (FeP , Fe_2P , and Fe_3P) were contaminated with molybdenum, tungsten, and rhenium after melting (see Figures S1–S3 in the supporting information) which is consistent with high-pressure studies of liquid Fe-S (Pommier, 2018). Before melting, no diffusion of Mo, W, and Re element is detected in specimens recovered from high pressure and temperature (Figure S2). Although studies demonstrated that the effect of molybdenum on the bulk electrical resistivity of the samples appears to be small (Pommier, 2018), we only use three resistance data after melting (100 K), in order to decrease the influence of contamination on data analyses.

3. Results and Discussions

The measured resistivity of a pure iron wire at 1.1 GPa is shown in Figure 3a, along with the ambient pressure data (Chu & Chi, 1981) and previous high-pressure results (Kiarasi, 2013; Secco & Schloessin, 1989; Silber et al., 2018). An inflection of the curve of the iron's resistivity is found around 1043 K, which is within a couple degrees of the Curie temperature (T_C) of pure iron at 1 atm (Chu & Chi, 1981). At $T < T_C$, the electrical resistivity of solid iron exhibits the expected T^2 dependence, which is in good agreement with the previous study (Yousuf et al., 1986). The resistivity of γ -Fe decreases with increasing pressures (Figure 3a).

3.1. Effects of T and P on the Resistivity of Iron Phosphide

As reported in previous high-pressure studies using diamond-anvil-cell techniques, no phase transition is observed for these three iron phosphides below 3 GPa (Dera et al., 2008; Gu et al., 2011, 2014). Thus, we only considered the effect from temperatures on the electrical resistivity at 1.3 to 3.2 GPa. The temperature dependences of electrical resistivity for three solid iron phosphide minerals (FeP , Fe_2P , and Fe_3P) at the pressures

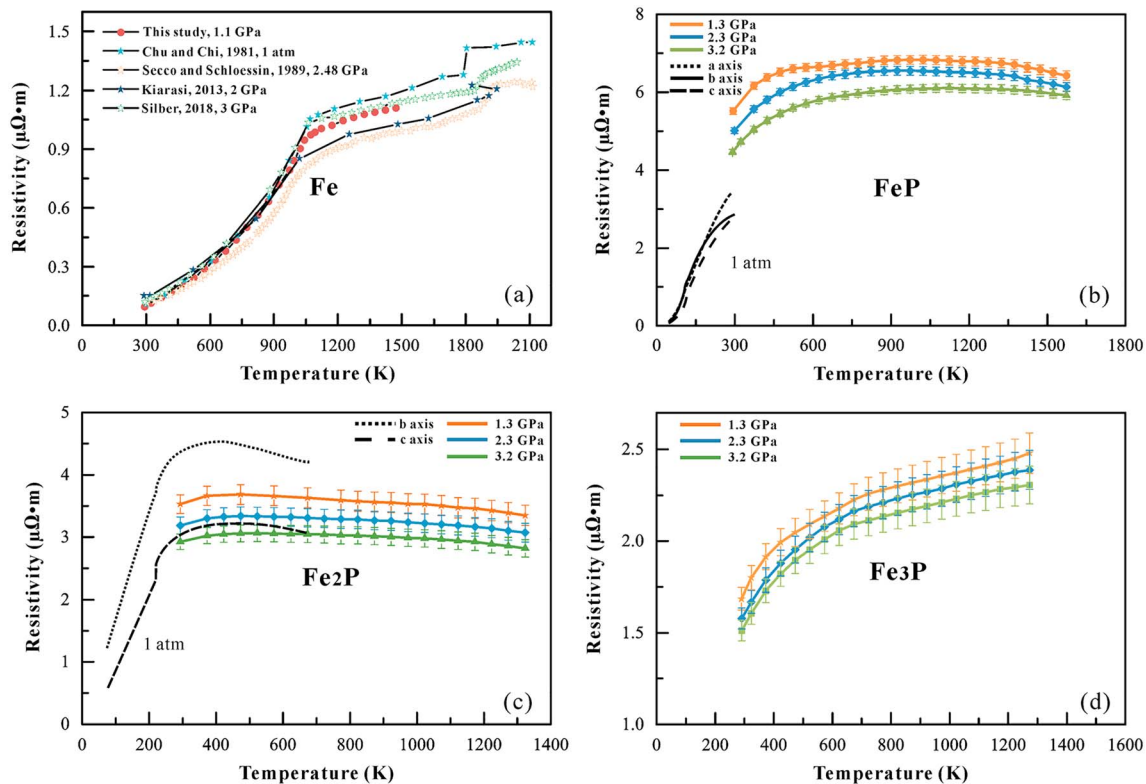


Figure 3. (a) The temperature dependence of electrical resistivity of solid iron at 1.1 GPa compared with 1 atm by Chu and Chi (1981), 2 GPa by Kiarasi (2013), 2.48 GPa by Secco and Schloessin (1989), and 3 GPa by Silber et al. (2018). (b) The temperature dependence of electrical resistivity of solid FeP at 1.3 to 3.2 GPa compared with 1 atm for single crystalline FeP with different axis reported by Westerstrandh et al. (1977). (c) The temperature dependence of electrical resistivity of solid Fe₂P at 1.3 to 3.2 GPa. Black solid lines are the resistivity of b and c axis of Fe₂P single crystalline at 1 atm (Fujii et al., 1977). (d) The electrical resistivity of solid Fe₃P at 1.3 to 3.2 GPa.

up to 3.2 GPa are shown in Figures 3b–3d, respectively. FeP had the highest resistivity as 4 to 7 $\mu\Omega\cdot\text{m}$ at temperatures up to 1600 K. With increasing temperature the resistivity of FeP increases rapidly to the highest value and decreases slightly at high T condition (>1200 K). A small negative slope for the trend of resistivity of solid Fe₂P was observed in this study, which is consistent with a previous result reported at 1 atm (Fujii et al., 1977). The resistivity of solid Fe₃P at 1 to 3 GPa is very similar to that of pure iron. It first increases rapidly with increasing temperature till the Curie temperature, and then increase linearly with a small slope (Figure 3d). As for the influence from phosphorus content on the resistivity, Fe₃P has the lowest electrical resistivity among three iron phosphides at 1.5 to 2.5 $\mu\Omega\cdot\text{m}$. It indicates that higher phosphorus content will lead to higher electrical resistivity in Fe-P system.

Previous studies indicate that the electrical resistivity of the solid metal and iron alloys (Fe-Si, Fe-C) decreases linearly with increasing pressures (Deng et al., 2013; Ezenwa & Secco, 2017a, 2017b; Kiarasi & Secco, 2015; Silber et al., 2017; Zhang et al., 2018). Similar behavior was also observed for iron phosphides in this study (Figure 4). More specifically, pressure has different influence on the resistivity for three iron phosphides at the pressure range of 1.3–3.2 GPa. Pressure coefficients for the electrical resistivity of three iron phosphides, $(d\ln\rho/dP)_T$ were calculated from the ρ versus P slopes. We used the data from 573 to 1273 K. Fe₂P has the largest pressure coefficient, while the resistivity of Fe₃P is slightly affected by pressure. The pressure coefficients for FeP, Fe₂P, and Fe₃P at 1273 K were $-0.053(1)$, $-0.086(2)$, and $-0.036(1)$, respectively.

3.2. Curie Temperatures of Fe₃P

An inflection point for the Fe₃P resistivity curve was found at $T = 723 \pm 25$ K which is likely T_C of this compound. Previous reports for T_C of Fe₃P at 1 atm is 716 (Meyer & Cadeville, 1962) and 686 K (Fruchart et al.,

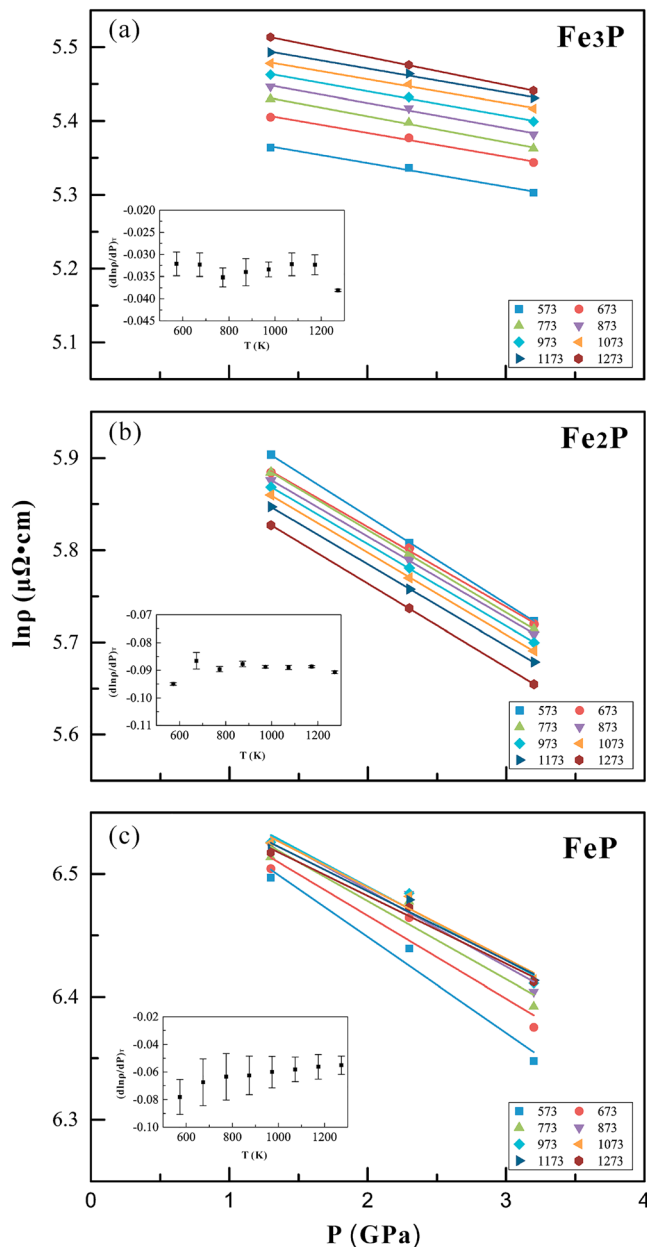


Figure 4. Pressure dependence of electrical resistivity of (a–c) three iron phosphides along 573–1271 K isotherms. Error bars are not shown here. The calculated slopes of the fitted lines, $(d\ln\rho/dP)_T$, are plotted in the insets at corresponding temperatures.

1964) where Fe_3P changes from ferromagnetic to paramagnetic. Usually, the resistivity of magnetic materials is made up of three terms associated with phonons, residual resistivity, and magnetic resistivity (Pepperhoff & Acet, 2001). The resistance from phonons (lattice vibrations), ρ_{ph} is temperature dependent and linear at high temperatures (above the Debye temperature). In magnetic metals, scattering of the conduction electrons occurs from the unpaired d-electrons, which are the carriers of the magnetic moment. The magnetic resistivity ρ_{mag} is maximum and constant in the paramagnetic state where the spins are randomly oriented. In Figure 3d, the electrical resistivity of Fe_3P above the Curie temperature behaves like paramagnetic metal, which has linear temperature dependence on the resistivity, and the slope equals to the ρ_{ph} . Different from pure iron, no typical T^2 dependence of resistivity is seen in Fe_3P below the Curie temperature. They have different magnetic structure (Goto et al., 1977; Liu et al., 1998) and result in different ρ_{mag} . Single crystalline Fe_3P has a tetragonal structure that will result in different resistivity along with ab axis and c axis. Our samples are polycrystalline. The anisotropy and orientation will lead to nontypical T^2 dependence of resistivity in ferromagnetic Fe_3P (Figure 3d).

3.3. Electrical Resistivity of FeP and Fe_2P Compared With 1 atm

It is noted that the resistivity of FeP and Fe_2P measured in this study at room temperature and 1.3 to 3.2 GPa is higher than that of single crystal obtained at ambient conditions (Figures 3b and 3c). The slightly higher resistivity for iron phosphides in this study is perhaps due to the synthesized polycrystalline samples. For crystalline iron phosphides samples, they have extraordinary high anisotropy along with different axis in the paramagnetic region (Figures 3b and 3c). Also, the grain size of samples may affect the resistivity. Our starting materials are sintered under high pressure and the average grain size is $<5 \mu\text{m}$ measured by scanning electron microscopy (Figure S4). It is hard to investigate the grain average axial orientation on the samples, but the anisotropy and grain size in the synthesized samples may lead to higher resistivity than crystalline samples. Another factor that may affect resistivity is hydrostaticity during compression. We used a similar pressure medium as Silber et al. (2017, 2018): hard Al_2O_3 plus boron nitride. Notably, the Curie temperatures and the pressure derivative of the resistance for Ni in Silber et al. (2017) are larger than the results from Sundqvist (1988) and Decker and Chen (1992) who used liquid pressure medium (petroleum ether and silicone oil, respectively) to provide hydrostatic condition. Decker and Chen (1992) argued that nonhydrostatic pressure environment or quasi-hydrostatic solid medium may lead to a higher slope on the Curie temperature versus pressure. For electrical resistivity of solid iron at high pressures, different results are observed in different works (Silber et al., 2018), which may be attributed to the different pressure medium used in their experiments.

Whereas the electrical resistivity of Fe_3P and pure iron increase steadily above T_c (Figures 3a and 3d), the electrical resistivity of both FeP and Fe_2P decreases after reaching a peak in the high-temperature region. FeP and Fe_2P are antiferromagnetic and paramagnetic at ambient conditions (Fujii et al., 1977; Westerstrandh et al., 1977), respectively. A first-order transition from metal to semiconductor takes place at Curie temperature (208.6 K) for Fe_2P at 1 atm (Figure 3c, Fujii et al., 1977). For semiconductor Fe_2P , the carrier concentration reaches saturation at high temperature and results in decreasing of electrical resistivity. FeP is also a semiconductor and has similar behavior with Fe_2P at high temperature.

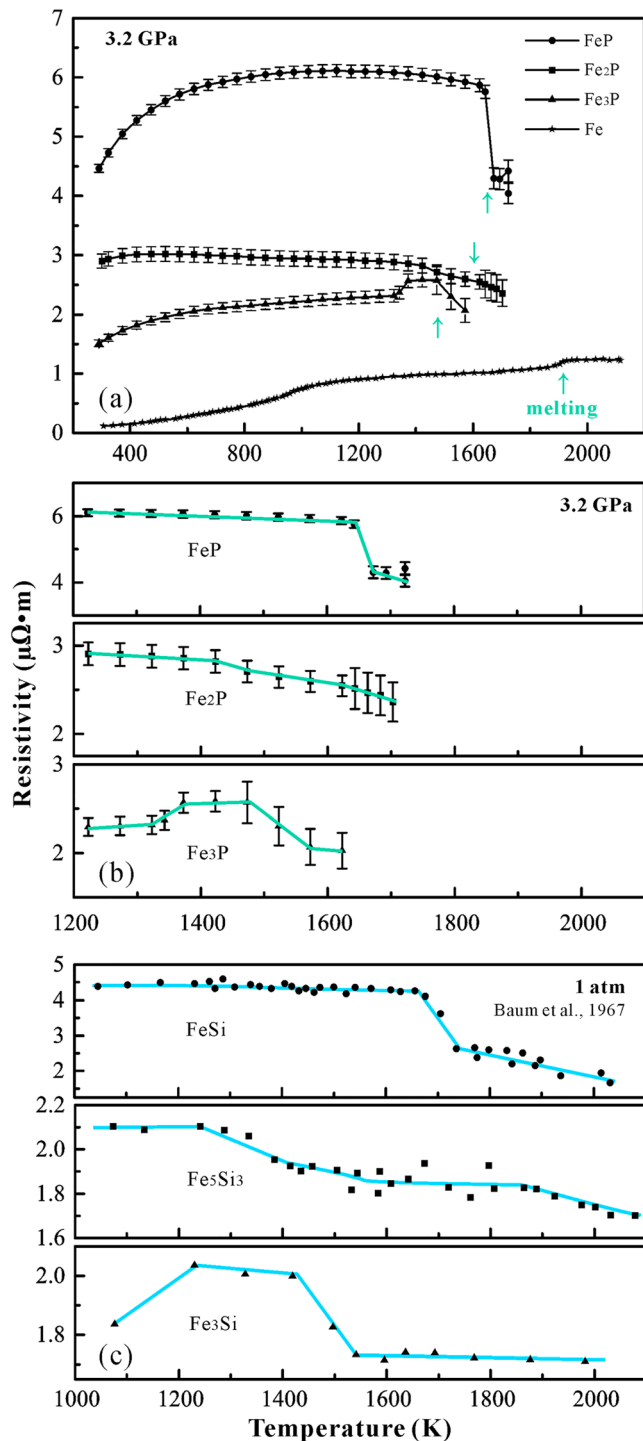


Figure 5. (a) Effect of temperature on the electrical resistivity of solid and liquid iron phosphides at 3.2 GPa. The experiment data for pure iron was measured at 2.48 GPa, by Secco and Schloessin (1989). (b) A close-up to the melting area. (c) The electrical resistivity for ferrosilicon alloys at 1 atm (Baum et al., 1967). Colored solid lines represent the trends of resistivity.

3.4. Electrical Resistivity of the Fe-P Melts

At the melting temperature, a distinct drop in the resistivity happened to FeP, Fe₂P, and Fe₃P, marked with arrows in Figure 5a. Thereafter, the resistivity for the Fe₂P and Fe₃P melt continuously decreased linearly with increasing temperatures. The same trend was also observed for iron silicide at 1 atm in the previous study (Baum et al., 1967; Figure 5c). Baum et al. (1967) also suggest that covalent bond between Fe and Si in the solid is broken at high temperatures, releasing Fe bound electrons which consequently decrease the resistivity. Although iron phosphides have different crystal structures than iron silicide, phosphorus atoms in the FeP, Fe₂P, and Fe₃P are also bonded covalently to iron. Hence, the resistivity decreases on melting may be due to the breaking of covalent bonds.

For Fe₂P, the slope of resistivity first changed at 1448 K, caused by the peritectic reaction, Fe₂P + Liquid \leftrightarrow Fe₃P. Above 1673 K, the resistivity decreased sharply due to the full melt of Fe₂P. These two changes were consistent with the Fe-P phase diagram at 1 atm by Okamoto (1990) and Zaitsev et al. (1995). This trend is similar with the behavior of Fe₅Si₃ (Figure 5c). Notably, the resistivity of Fe₃P first jump from 2.32 $\mu\Omega\cdot m$ at 1323 K to 2.57 $\mu\Omega\cdot m$ at 1373 K which is very close to the eutectic temperature 1321 K at 1 atm (Okamoto, 1990), 1358 K at 3 GPa (Yin et al., 2019), and 1348 K at 6 GPa (Minin et al., 2019). Above that temperature, a small amount of melt becomes thermodynamically stable and coexists with solid Fe₃P. The melt is composed of ~ 90 wt% Fe and ~ 10 wt% P (Okamoto, 1990), has a more disordered structure and higher electrical resistivity than solid, thus causing the first jump we observe in the electrical resistivity of Fe₃P. Above 1448 K, the resistivity of Fe₃P drops from 2.57 $\mu\Omega\cdot m$ at 1473 K to 2.07 $\mu\Omega\cdot m$ at 1573 K. The melting temperature of Fe₃P is 1439 K (Okamoto, 1990; Zaitsev et al., 1995) at 1 atm and 1458 K at 3 GPa (Yin et al., 2019). Thus, the drop should result from the breaking of Fe-P bonds at its melting temperature. This behavior is consistent with Fe₃Si at its melting point (Figure 5c). The slope of the resistivity versus temperature in liquid Fe₃P is slightly negative ($T > 1573$ K). Figure 6 shows that melting temperatures are 1643 ± 25 K for FeP, 1623 ± 25 K for Fe₂P, and 1473 ± 25 K for Fe₃P at 3.2 GPa, which are consistent with the melting points at 1 atm (Zaitsev et al., 1995).

4. Alloying Effect of Light Elements (P, C, and Si) on the Resistivity of Fe

The effect of carbon on the thermal conductivity of iron was reported very recently (Zhang et al., 2018). The resistivity of Fe-C system, including iron, Fe₉₉C₁ alloy (contains 0.2 wt% carbon), Fe₃C, and Fe₇C₃, have been measured at room temperature and up to 80 GPa by using diamond anvil cell. Fe-C alloy performed an exceedingly stronger alloying effect than Si, S, and Ni. When the same content of light element was added in the iron, Fe-C alloy has the highest electrical resistivity among Fe-P and Fe-Si alloys (Figure 7a). Pommier (2018) reported the electrical resistivity of Fe-S mixtures and its melts, which shows extremely larger values than pure iron. That work should not represent the accurate impurity resistivity of sulfur in the solid Fe-S alloy, because it is just a combination of two

materials. The experimentally measured resistivity of Fe-Si system exhibits two trends with increasing Si content due to the presence of atomic order-disorder (Numakura et al., 1972; Ruiz et al., 2005; Varga et al., 2002). One trend shows a resistivity rise with Si content and the second trend shows a significant

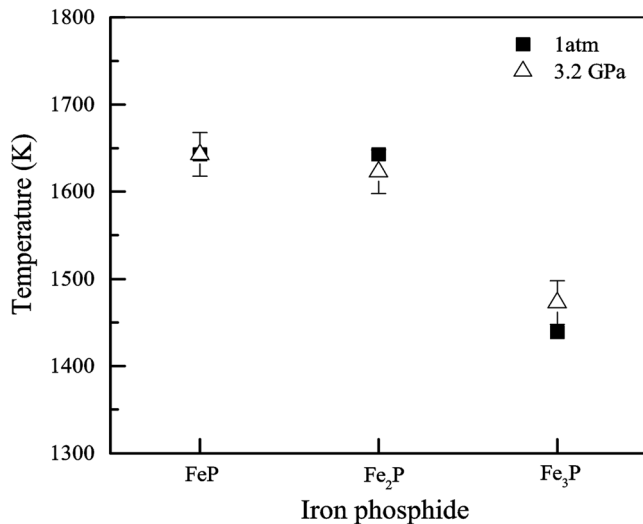


Figure 6. Melting temperatures for different iron phosphides at 3.2 GPa in this study compared with results at 1 atm (Zaitsev et al., 1995).

decrease in resistivity beginning at 10 wt% Si, reaching a minimum at 15 wt% Si, followed by an increase in resistivity with Si content up to 20 wt% where this trend joins the first trend (Figure 7a). Fe-P alloys seem to have the same trend that a minimum resistivity exists at Fe₃P along with a linear relationship between iron, FeP, and Fe₂P. Even though FeP and Fe₂P have ordered structures, their resistivity is still on the trend of disordered Fe-P alloy at high phosphorus region, which is comparable with the first trend of Fe-Si system (Figure 7b).

To describe the “ideal” total resistivity of a dilute iron alloy, Matthiessen’s rule (Matthiessen & Vogt, 1864) is often used in previous studies (Seagle et al., 2013; Zhang et al., 2018), defined as the following form:

$$\rho_{Fe-i}(V, T) = \rho_{Fe}(V, T) + \rho_i(V) \times x_i \quad (3)$$

where i represents the alloying elements, $\rho_i(V)$ is the compositional dependent unit resistivity, and x_i is the content of the alloying element in atomic percent (at.%), $\rho_{Fe-i}(V, T)$ is the total resistivity of the iron alloys, and $\rho_{Fe}(V, T)$ is the resistivity of pure iron as a function of pressure and temperature. The second part of this formula ($\rho_i(V)$) is called impurity resistivity and only depends on the volume (corresponding to pressures).

Matthiessen’s rule clearly demonstrates the linear correlation between the alloying element’s concentration and the alloy’s resistivity at a fixed P and T condition. This rule is confirmed by experimental results from Fe-Si, Fe-C, and Fe-P alloys at 1 atm and room temperature, as shown in Figure 7b. The resistivity for Fe-P alloy is linear with phosphorus content (P, 0–3.4 at.%) at ambient condition (Węgliński & Kaczmar, 1980), which agrees with the prediction of Matthiessen’s rule. In some scenarios, Matthiessen’s rule will break down due to “saturation effect” caused by chemical composition (Gomi et al., 2016), pressure (Kiarasi & Secco, 2015), and temperatures (Pozzo & Alfè, 2016). Also, Wagle et al. (2018) observed that the temperature coefficient of resistivity for liquid Fe-S system changes from positive to negative at high compression and high sulfur concentration. In that case, Matthiessen’s rule is invalid to model the electrical resistivity of Fe-L alloys. But, it is no doubt that Matthiessen rule is reasonable here to describe the electrical resistivity of solid Fe-P alloys at a moderate pressure condition (≤ 5 GPa).

For α -Fe, its electrical resistivity does not change a lot at room temperature and below 5 GPa (Gomi et al., 2013; Secco & Schloessin, 1989; Silber et al., 2018; Zhang et al., 2018). Thus, we fix the $\rho_{Fe}(V, T)$ at 9.44 $\mu\Omega\cdot\text{cm}$ measured at 1.1 GPa in this study. According to the measured resistivity for FeP and Fe₂P, we

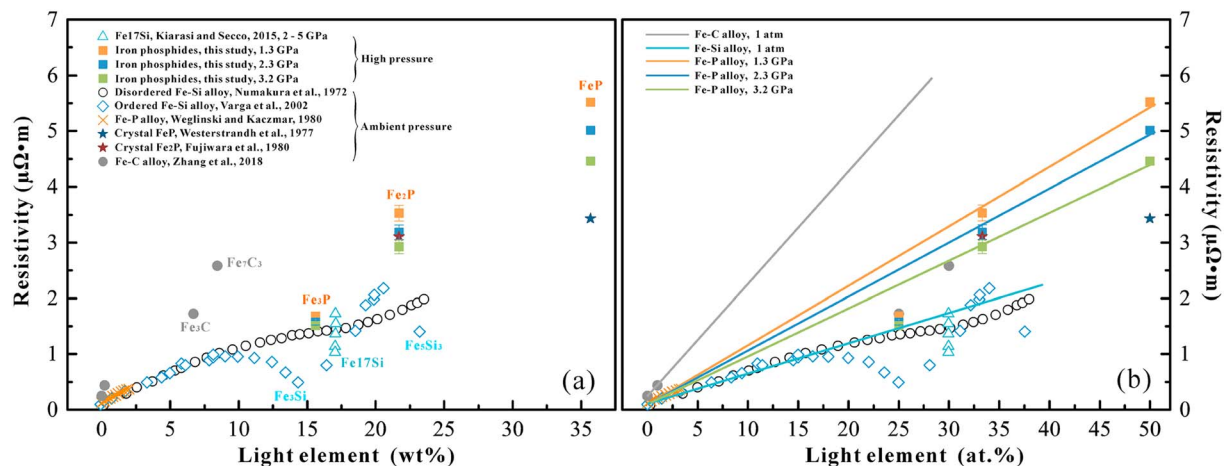


Figure 7. Dependence of electrical resistivity for Fe-L compounds with different contents of light elements at room temperature. (a) and (b) are weight and atomic percent, respectively. The resistivity of Fe17Si (17 wt% Si) was measured by Kiarasi and Secco (2015) at the pressures of 2–5 GPa. Colorful solid lines in (b) represent the fit of resistivity data for disordered alloy (Fe-C, Fe-P, and Fe-Si) according to Matthiessen’s rule.

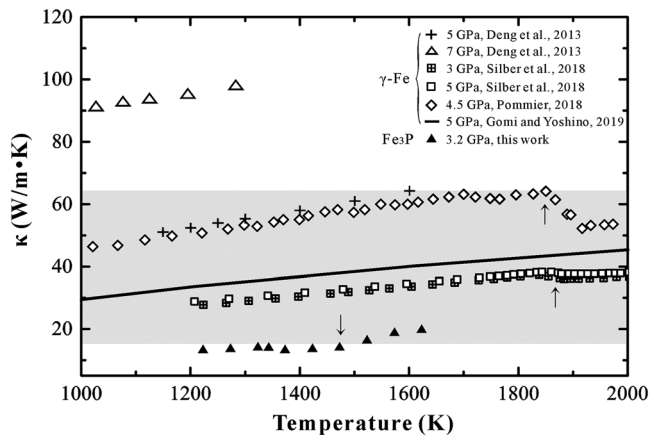


Figure 8. Temperature dependence of thermal conductivity for γ -Fe and Fe_3P at 3–5 GPa. Error bars are smaller than symbols. Arrows indicate the melting point. Gray region represents an estimated limit of lunar core's thermal conductivity.

calculate the ρ_i (V) for phosphorus at pressures of 1.3, 2.3, and 3.2 GPa, resulting in 10.68, 9.67, and 8.67 ($\mu\Omega\text{-cm/at } \%$), respectively (Figure 7b). Also, we can see that phosphorus has higher impurity resistivity than silicon and lower than carbon. It is in agreement with the study of Gomi and Yoshino (2018) who discussed this impurity resistivity trend in *fcc* and *hcp* iron for light element candidates (C, N, O, Si, and S). The impurity resistivity increases with increasing atomic number in the same period. In the same group, the second period atoms show higher impurity resistivity than third period atoms, which is consistent with the experimental fact of C (Zhang et al., 2018) and Si (Gomi et al., 2016) in *hcp* iron.

5. Implication for the Thermal Conductivity of Lunar Core

The moon has a small metallic core according to numerous geophysical and geochemical studies (Righter, 2002; Weber et al., 2011; Williams et al., 2001, 2014; Zuber et al., 2011). Assuming different lunar core composition, the core size can be satisfied by either a ~330-km radius solid iron core or ~460-km radius liquid eutectic Fe-FeS core (Wieczorek, 2006). The lunar core is assumed to be composed by a solid inner and liquid outer core which contains a large range of S content of 2–20 at.% (corresponding to 1–11 wt%; Antonangeli et al., 2015; Jing et al., 2014; Kuwabara et al., 2016; Morard et al., 2018; Righter et al., 2017; Weber et al., 2011). However, a recent study argued that the lunar core should not be S-rich but C-rich by the evidence of light element partition between the metal core and silicate Moon (Steenstra et al., 2017). Notably, phosphorus has large solubility (up to 10 wt%, corresponding to ~17 at.%) in the liquid iron and liquid Fe-S-P alloys (Stewart & Schmidt, 2007; Zaitsev et al., 1995), which means considerable phosphorus could be present in the core. A wide speculation to the state of the lunar core gives that current temperature at CMB could be between ~1473 K (Chacko & De Bremaecker, 1982; Scheinberg et al., 2015; Ziethe et al., 2009) and 1650 K (Spohn et al., 2001), even as high as ~1773 K (Laneuville et al., 2014; Scheinberg et al., 2015; Zhang et al., 2013), and the core pressure could be 4.5 to 5.5 GPa (Antonangeli et al., 2015; Kuskov & Kronrod, 1998). At such temperature and pressure conditions, the thermal conductivity of the lunar core has not been investigated intensively.

The thermal conductivity (k) for the iron and Fe-L alloy can be calculated by the electrical resistivity using the Wiedemann-Franz law:

$$k = LT/\rho \quad (4)$$

where k , L , T , and ρ are the thermal conductivity (W/m·K), Lorenz number (ideal value, 2.44×10^{-8} W· Ω /K²), the absolute temperature, and the electrical resistivity ($\Omega\text{-m}$), respectively. The Lorenz number is believed to be variable with the temperatures and pressures and well discussed through theoretical calculations (de Koker et al., 2012; Pozzo et al., 2013) and experimental studies on the Seebeck coefficient of iron (Secco, 2017). However, to be comparative with previous studies (Gomi et al., 2013, 2016; Gomi & Hirose, 2015; Ohta et al., 2016; Pommier, 2018; Seagle et al., 2013; Suehiro et al., 2017; Zhang et al., 2018), we use the ideal value here to calculate the thermal conductivity of Fe-P system.

The thermal conductivity against temperature for Fe_3P at high temperatures and 3.2 GPa are calculated and shown in Figure 8. Fe_3P has a low thermal conductivity of ~10 to 20 W/m·K due to its high electrical resistivity. For comparison, we used the electrical resistivity for γ -Fe measured by Silber et al. (2018) at 3 and 5 GPa and calculated by Gomi and Yoshino (2019) at 5 GPa to estimate the thermal conductivity of γ -Fe at 1000–2000 K. The thermal conductivity calculated by Deng et al. (2013) and Pommier (2018) are also plotted in Figure 8. It is obvious that previous measurements have a large variation within the γ -Fe stability field at 3 to 5 GPa. All three studies use a four-wire method in the multianvil apparatus, to determine electrical resistivity for solid γ -Fe at 3–5 GPa and 1000–2000 K. The results of Deng et al. (2013) and Pommier (2018) are very similar to each other but significantly different from the result by Silber et al. (2018). Using first principle calculation, Gomi and Yoshino (2019) calculated similar electrical resistivity for γ -Fe at 5 GPa to that measured by Silber et al. (2018). Thus, the thermal conductivity for γ -Fe at 5 GPa and 1000–2000 K has a

large range from 28 to 64 W/m-K (Figure 8). However, in many models, lunar core's thermal conductivity was generally set at a moderate value of 50 W/m-K (Laneuville et al., 2014; Zhang et al., 2013), which was calculated by first-principles electronic structure computations for iron and iron-silicon system (de Koker et al., 2012). Silber et al. (2018) calculated the thermal conductivity of the lunar core as 33.5 W/m-K. That value should be used with caution because the lower electrical resistivity for γ -Fe at 5 GPa calculated by Gomi and Yoshino (2019) supports a higher thermal conductivity for the lunar core (Figure 8).

For the accurate situation of the lunar core, these values (50 and 33.5 W/m-K) might be slightly overestimated due to the amount of potential light elements stored in the core (Jing et al., 2014; Richter et al., 2017). Assuming the lunar core has a significant amount of phosphorus, a Fe-P core (similar with Fe-Si, Fe-C, and Fe-S alloys) has higher electrical resistivity and lower thermal conductivity than a pure iron core model (Figure 8). With increasing pressure, the resistivity of solid iron and iron alloy decreases, yielding higher thermal conductivity. It is hard to say their melts may follow the same rule because experiments show that the electrical resistivity is invariant at the melting points of Fe at 6–12 GPa (Silber et al., 2018), Ni up to 9 GPa (Silber et al., 2017), and Co up to 5 GPa (Ezenwa & Secco, 2017b). The thermal conductivity of solid Fe₃P at ~5 GPa should be slightly higher than the calculation in Figure 8. According to phase diagram, potential Fe-L compounds in the lunar solid inner core should be Fe₃P (Chantel et al., 2018; Minin et al., 2019; Yin et al., 2019), Fe₃C (Fei & Brosh, 2014), and Fe₃Si (Ohnuma et al., 2012). Also, theoretical calculations demonstrate that Fe₃P is stable and ferromagnetic to at least 200 GPa (Zhao et al., 2017). The ordered compounds Fe₃P and Fe₃C have a close electrical resistivity and quite larger than the ordered Fe₃Si (Figure 7a) and pure iron. When we look at the boundary at the solid inner and liquid outer cores in the Moon, a large gap or discontinuity in the thermal conductivity caused by Fe-L compounds (e.g., Fe₃P) would result in a special thermal regime at that boundary. Upon melting of the ordered compound Fe₃P, thermal conductivity increases about 33% due to the drop of the electrical resistivity caused by breaking of Fe-P covalent bonds.

6. Conclusions

The electrical resistivity of three Fe-P compounds (FeP, Fe₂P, and Fe₃P) has been measured at 1.3–3.2 GPa and up to 1800 K. Iron phosphides have higher impurity resistivity than silicon and lower impurity resistivity than carbon, which suggests that phosphorus has a strong alloying effect on the electrical resistivity of iron. Using the Wiedemann-Franz law, the thermal conductivity of Fe₃P was calculated at 1223 to 1623 K and 3.2 GPa. Due to the breaking of Fe-P bonds at the melting point, a drop on the resistivity may result in 33% increase in the thermal conductivity. That will lead to a discontinuity on the thermal state at the lunar solid inner core and liquid outer core.

Acknowledgments

All data supporting the conclusions of this paper can be found in the cited references, tables, and supporting information. We acknowledge anonymous Associate Editor and reviewers for their thorough review of this manuscript. We also thank Stephen Parman for the handling of this manuscript. We thank Kai Li for his help with the electrical resistivity measurement and Wen Liang for helpful discussion. We are grateful to Zachary Geballe for the improvement of the written English language. This work was financially supported by the National Natural Science Foundation of China (grant 41873073), the Western Light Talents Training Program of Chinese Academy of Sciences. The authors declare no competing financial interests.

References

- Abliz, M., Uwatoko, Y., Ohki, T., Fujii, H., & Secco, R. A. (2006). New pressure-induced phase transitions in Fe₂P. *Journal of the Physical Society of Japan*, 75(12), 123706. <https://doi.org/10.1143/JPSJ.75.123706>
- Antonangeli, D., Morard, G., Schmerr, N. C., Komabayashi, T., Krisch, M., Fiquet, G., & Fei, Y. (2015). Toward a mineral physics reference model for the Moon's core. *Proceedings of the National Academy of Sciences*, 112(13), 3916–3919. <https://doi.org/10.1073/pnas.1417490112>
- Baum, B. A., Gel'd, P. V., & Tyagunov, G. V. (1967). Resistivity of ferrosilicon alloys in the temperature range 800–1700 °C. *Physics of Metals and Metallography*, 24, 181–184.
- Britvin, S. N., Murashko, M. N., Vapnik, Y., Polekhovskiy, Y. S., & Krivovichev, S. V. (2015). Earth's phosphides in Levant and insights into the source of Archean prebiotic phosphorus. *Scientific Reports*, 5(1), 8355. <https://doi.org/10.1038/srep08355>
- Britvin, S. N., Rudashevskiy, N. S., Krivovichev, S. V., Burns, P. C., & Polekhovskiy, Y. S. (2002). Allabogdanite, (Fe,Ni)₂P, a new mineral from the Onello meteorite: The occurrence and crystal structure. *American Mineralogist*, 87(8–9), 1245–1249. <https://doi.org/10.2138/am-2002-8-924>
- Chacko, S., & De Bremaecker, J. C. (1982). The evolution of the moon: A finite element approach. *The Moon and the Planets*, 27(4), 467–492. <https://doi.org/10.1007/BF00930000>
- Chantel, J., Jing, Z., Xu, M., Yu, T., & Wang, Y. (2018). Pressure dependence of the liquidus and solidus temperatures in the Fe-P binary system determined by in situ ultrasonics: Implications to the solidification of Fe-P liquids in planetary cores. *Journal of Geophysical Research: Planets*, 123, 1113–1124. <https://doi.org/10.1029/2017JE005376>
- Chu, T. K., & Chi, T. C. (1981). *Properties of Selected Ferrous Alloying Elements* (III-1, 269 pp.). Washington: McGraw-Hill.
- de Koker, N., Steinle-Neumann, G., & Vlcek, V. (2012). Electrical resistivity and thermal conductivity of liquid Fe alloys at high P and T, and heat flux in Earth's core. *Proceedings of the National Academy of Sciences*, 109(11), 4070–4073. <https://doi.org/10.1073/pnas.1111841109>
- Decker, D. L., & Chen, W. (1992). High-precision measurement of electrical resistivity of nickel near the ferromagnetic phase transition at high pressure. *Physical Review B*, 46(13), 8237–8243. <https://doi.org/10.1103/PhysRevB.46.8237>

- Deng, L., Seagle, C., Fei, Y., & Shahar, A. (2013). High pressure and temperature electrical resistivity of iron and implications for planetary cores. *Geophysical Research Letters*, *40*, 33–37. <https://doi.org/10.1029/2012GL054347>
- Dera, P., Lavina, B., Borkowski, L. A., Prakapenka, V. B., Sutton, S. R., Rivers, M. L., et al. (2008). High-pressure polymorphism of Fe₂P and its implications for meteorites and Earth's core. *Geophysical Research Letters*, *35*, L10301. <https://doi.org/10.1029/2008GL033867>
- Desai, P. D., Chu, T. K., James, H. M., & Ho, C. Y. (1984). Electrical resistivity of selected elements. *Journal of Physical and Chemical Reference Data*, *13*(4), 1069–1096. <https://doi.org/10.1063/1.555723>
- Drake, M. J. (1987). Siderophile elements in planetary mantles and the origin of the Moon. *Journal of Geophysical Research*, *92*(B4), E377–E386. <https://doi.org/10.1029/JB092iB04p0E377>
- Ezenwa, I. C., & Secco, R. A. (2017a). Constant electrical resistivity of Zn along the melting boundary up to 5 GPa. *High Pressure Research*, *37*(3), 319–333. <https://doi.org/10.1080/08957959.2017.1340473>
- Ezenwa, I. C., & Secco, R. A. (2017b). Invariant electrical resistivity of Co along the melting boundary. *Earth and Planetary Science Letters*, *474*, 120–127. <https://doi.org/10.1016/j.epsl.2017.06.032>
- Fei, Y., & Brosh, E. (2014). Experimental study and thermodynamic calculations of phase relations in the Fe–C system at high pressure. *Earth and Planetary Science Letters*, *408*, 155–162. <https://doi.org/10.1016/j.epsl.2014.09.044>
- Fruchart, E., Triquet, A. M., & Fruchart, R. (1964). Magnetic studies of borophosphides of iron, Fe₃B_xP_{1-x} ε and ε₁. Notes on the metal bonds of the metal transitive-metalloid in these compounds. *Annales de Chimie (Paris)*, *9*(7–8), 323–332.
- Fujii, H., Hōkabe, T., Kamigaichi, T., & Okamoto, T. (1977). Magnetic properties of Fe₂P single crystal. *Journal of the Physical Society of Japan*, *43*(1), 41–46. <https://doi.org/10.1143/JPSJ.43.41>
- Fujiwara, H., Kadomatsu, H., Tohma, K., Fujii, H., & Okamoto, T. (1980). Pressure-induced magnetic transition in Fe₂P. *Journal of Magnetism and Magnetic Materials*, *21*(3), 262–268. [https://doi.org/10.1016/0304-8853\(80\)90470-9](https://doi.org/10.1016/0304-8853(80)90470-9)
- Gomi, H., & Hirose, K. (2015). Electrical resistivity and thermal conductivity of hcp Fe–Ni alloys under high pressure: Implications for thermal convection in the Earth's core. *Physics of the Earth and Planetary Interiors*, *247*, 2–10. <https://doi.org/10.1016/j.pepi.2015.04.003>
- Gomi, H., Hirose, K., Akai, H., & Fei, Y. (2016). Electrical resistivity of substitutionally disordered hcp Fe–Si and Fe–Ni alloys: Chemically-induced resistivity saturation in the Earth's core. *Earth and Planetary Science Letters*, *451*, 51–61. <https://doi.org/10.1016/j.epsl.2016.07.011>
- Gomi, H., Ohta, K., Hirose, K., Labrosse, S., Caracas, R., Verstraete, M. J., & Hernlund, J. W. (2013). The high conductivity of iron and thermal evolution of the Earth's core. *Physics of the Earth and Planetary Interiors*, *224*, 88–103. <https://doi.org/10.1016/j.pepi.2013.07.010>
- Gomi, H., & Yoshino, T. (2018). Impurity resistivity of fcc and hcp Fe-based alloys: Thermal stratification at the top of the core of super-Earths. *Frontiers in Earth Science*, *6*, 1–22. <https://doi.org/10.3389/feart.2018.00217>
- Gomi, H., & Yoshino, T. (2019). Electrical resistivity and thermal conductivity of fcc Fe: Implications for the Mercury's core. Joint symposium of Misasa 2019 & CMC: Origin, Evolution & Dynamics of the Earth & Planetary Interiors. https://www.misasa.okayama-u.ac.jp/symp/Misasa_CMC_abstracts.pdf
- Goto, M., Tange, H., Tokunaga, T., Fujii, H., & Okamoto, T. (1977). Magnetic properties of the (Fe_{1-x}M_x)₃P compounds. *Japanese Journal of Applied Physics*, *16*(12), 2175–2179. <https://doi.org/10.1143/JJAP.16.2175>
- Gu, T., Fei, Y., Wu, X., & Qin, S. (2014). High-pressure behavior of Fe₃P and the role of phosphorus in planetary cores. *Earth and Planetary Science Letters*, *390*, 296–303. <https://doi.org/10.1016/j.epsl.2014.01.019>
- Gu, T., Wu, X., Qin, S., & Dubrovinsky, L. (2011). In situ high-pressure study of FeP: Implications for planetary cores. *Physics of the Earth and Planetary Interiors*, *184*(3–4), 154–159. <https://doi.org/10.1016/j.pepi.2010.11.004>
- Gu, T., Wu, X., Qin, S., McCammon, C., & Dubrovinsky, L. (2013). Probing nonequivalent sites in iron phosphide Fe₂P and its mechanism of phase transition. *The European Physical Journal B*, *86*(7), 311. <https://doi.org/10.1140/epjb/e2013-40086-3>
- Jing, Z., Wang, Y., Kono, Y., Yu, T., Sakamaki, T., Park, C., et al. (2014). Sound velocity of Fe–S liquids at high pressure: Implications for the Moon's molten outer core. *Earth and Planetary Science Letters*, *396*, 78–87. <https://doi.org/10.1016/j.epsl.2014.04.015>
- Kiarasi, S. (2013). High pressure-temperature electrical resistivity experiments on Fe–Si alloys bearing on conductive heat flow at the top of the outer core. Electronic Thesis and Dissertation Repository. 1793, 43–45. Retrieved from. <https://ir.lib.uwo.ca/etd/1793>
- Kiarasi, S., & Secco, R. A. (2015). Pressure-induced electrical resistivity saturation of Fe₁₇Si. *Physica Status Solidi B*, *252*(9), 2034–2042. <https://doi.org/10.1002/pssb.201552029>
- Konôpková, Z., McWilliams, R. S., Gómez-Pérez, N., & Goncharov, A. F. (2016). Direct measurement of thermal conductivity in solid iron at planetary core conditions. *Nature*, *534*(7605), 99–101. <https://doi.org/10.1038/nature18009>
- Kuskov, O., & Kronrod, V. (1998). Constitution of the Moon. *Physics of the Earth and Planetary Interiors*, *107*(4), 285–306. [https://doi.org/10.1016/S0031-9201\(98\)00082-X](https://doi.org/10.1016/S0031-9201(98)00082-X)
- Kuwabara, S., Terasaki, H., Nishida, K., Shimoyama, Y., Takubo, Y., Higo, Y., et al. (2016). Sound velocity and elastic properties of Fe–Ni and Fe–Ni–C liquids at high pressure. *Physics and Chemistry of Minerals*, *43*(3), 229–236. <https://doi.org/10.1007/s00269-015-0789-y>
- Laneuville, M., Wieczorek, M. A., Breuer, D., Aubert, J., Morard, G., & Rückriemen, T. (2014). A long-lived lunar dynamo powered by core crystallization. *Earth and Planetary Science Letters*, *401*, 251–260. <https://doi.org/10.1016/j.epsl.2014.05.057>
- Liu, H., James, P., Brodbeck, A., Andersson, Y., Granberg, P., & Eriksson, O. (1998). Structural and magnetic properties of (Fe_{1-x}Co_x)₃P compounds: experiment and theory. *Journal of Magnetism and Magnetic Materials*, *189*(1), 69–82. [https://doi.org/10.1016/S0304-8853\(98\)00203-0](https://doi.org/10.1016/S0304-8853(98)00203-0)
- Matthiessen, A., & Vogt, C. (1864). On the influence of temperature on the electric conducting-power of alloys. *Philosophical Transactions of the Royal Society of London*, *154*, 167–200. <https://doi.org/10.1098/rstl.1864.0004>
- McDonough, W. F. (2003). Compositional model for the Earth's core. In K. K. Turekian, & H. D. Holland (Eds.), *Treatise on Geochemistry*, (1st ed., pp. 547–568). Amsterdam: Elsevier Ltd. <https://doi.org/10.1016/B0-08-043751-6/02015-6>
- McDonough, W. F., & Sun, S. (1995). The composition of the Earth. *Chemical Geology*, *120*(3–4), 223–253. [https://doi.org/10.1016/0009-2541\(94\)00140-4](https://doi.org/10.1016/0009-2541(94)00140-4)
- Meyer, A. J. P., & Cadeville, M. C. (1962). Magnetic properties of iron-phosphorus compounds. *Journal of the Physical Society of Japan*, *17*, 223–225.
- Minin, D. A., Shatskiy, A. F., Litasov, K. D., & Ohfuiji, H. (2019). The Fe–Fe₂P phase diagram at 6 GPa. *High Pressure Research*, *39*(1), 50–68. <https://doi.org/10.1080/08957959.2018.1562552>
- Morard, G., Bouchet, J., Rivoldini, A., Antonangeli, D., Roberge, M., Boulard, E., et al. (2018). Liquid properties in the Fe–FeS system under moderate pressure: Tool box to model small planetary cores. *American Mineralogist*, *103*, 1770–1779. <https://doi.org/10.2138/am-2018-6405>

- Newsom, H. E. (1990). Accretion and core formation in the Earth: Evidence from siderophile elements. In *Origin of the Earth* (pp. 273–288). LPI Conference on the Origin of the Earth.
- Newsom, H. E. (1995). Composition of the solar system, planets, meteorites, and major terrestrial reservoirs. In *Global Earth Physics a handbook of physical constants*, (pp. 159–189). Washington, DC: American Geophysical Union. <https://doi.org/10.1029/RF001p0159>
- Newsom, H. E., & Drake, M. J. (1983). Experimental investigation of the partitioning of phosphorus between metal and silicate phases: Implications for the Earth, Moon and Eucrite Parent Body. *Geochimica et Cosmochimica Acta*, *47*(1), 93–100. [https://doi.org/10.1016/0016-7037\(83\)90093-5](https://doi.org/10.1016/0016-7037(83)90093-5)
- Newsom, H. E., & Taylor, S. R. (1989). Geochemical implications of the formation of the Moon by a single giant impact. *Nature*, *338*(6210), 29–34. <https://doi.org/10.1038/338029a0>
- Numakura, K., Tsugawa, A., Sugano, M., & Sato, Y. (1972). Magnetic and electric properties of Fe-silicon alloys. *Science Reports of the Research Institutes, Tohoku University. Ser. A, Physics, Chemistry and Metallurgy*, *24*, 48–60. <http://hdl.handle.net/10097/00102972>
- Ohnuma, I., Abe, S., Shimenuchi, S., Omori, T., Kainuma, R., & Ishida, K. (2012). Experimental and thermodynamic studies of the Fe–Si binary system. *ISIJ International*, *52*(4), 540–548. <https://doi.org/10.2355/isijinternational.52.540>
- Ohta, K., Kuwayama, Y., Hirose, K., Shimizu, K., & Ohishi, Y. (2016). Experimental determination of the electrical resistivity of iron at Earth's core conditions. *Nature*, *534*(7605), 95–98. <https://doi.org/10.1038/nature17957>
- Okamoto, H. (1990). The Fe–P (iron–phosphorus) system. *Bulletin of Alloy Phase Diagrams*, *11*(4), 404–412. <https://doi.org/10.1007/BF02843320>
- Pepperhoff, W., & Acet, M. (2001). *Constitution and magnetism of iron and its alloys*. Berlin Heidelberg: Springer-Verlag. <https://doi.org/10.1007/978-3-662-04345-5>
- Pommier, A. (2018). Influence of sulfur on the electrical resistivity of a crystallizing core in small terrestrial bodies. *Earth and Planetary Science Letters*, *496*, 37–46. <https://doi.org/https://doi.org/10.1016/j.epsl.2018.05.032>
- Pozzo, M., & Alfè, D. (2016). Saturation of electrical resistivity of solid iron at Earth's core conditions. *Springerplus*, *5*(1), 256–256. <https://doi.org/10.1186/s40064-016-1829-x>
- Pozzo, M., Davies, C., Gubbins, D., & Alfè, D. (2012). Thermal and electrical conductivity of iron at Earth's core conditions. *Nature*, *485*(7398), 355–358. <https://doi.org/10.1038/nature11031>
- Pozzo, M., Davies, C., Gubbins, D., & Alfè, D. (2013). Transport properties for liquid silicon–oxygen–iron mixtures at Earth's core conditions. *Physical Review B: Condensed Matter and Materials Physics*, *87*(1), 1–10. <https://doi.org/10.1103/PhysRevB.87.014110>
- Pratesi, G. (2006). Icosahedral coordination of phosphorus in the crystal structure of melilinite, a new phosphide mineral from the northwest Africa 1054 acapulcoite. *American Mineralogist*, *91*(2–3), 451–454. <https://doi.org/10.2138/am.2006.2095>
- Righter, K. (2002). Does the Moon have a metallic core? Constraints from giant impact modeling and siderophile elements. *Icarus*, *158*(1), 1–13. <https://doi.org/10.1006/icar.2002.6859>
- Righter, K. (2003). Metal–silicate partitioning of siderophile elements and core formation in the early Earth. *Annual Review of Earth and Planetary Sciences*, *31*(1), 135–174. <https://doi.org/10.1146/annurev.earth.31.100901.145451>
- Righter, K., & Chabot, N. L. (2011). Moderately and slightly siderophile element constraints on the depth and extent of melting in early Mars. *Meteoritics and Planetary Science*, *46*(2), 157–176. <https://doi.org/10.1111/j.1945-5100.2010.01140.x>
- Righter, K., Drake, M. J., & Yaxley, G. (1997). Prediction of siderophile element metal–silicate partition coefficients to 20 GPa and 2800 °C: the effects of pressure, temperature, oxygen fugacity, and silicate and metallic melt compositions. *Physics of the Earth and Planetary Interiors*, *100*(1–4), 115–134. [https://doi.org/10.1016/S0031-9201\(96\)03235-9](https://doi.org/10.1016/S0031-9201(96)03235-9)
- Righter, K., Go, B. M., Pando, K. A., Danielson, L., Ross, D. K., Rahman, Z., & Keller, L. P. (2017). Phase equilibria of a low S and C lunar core: Implications for an early lunar dynamo and physical state of the current core. *Earth and Planetary Science Letters*, *463*, 323–332. <https://doi.org/10.1016/j.epsl.2017.02.003>
- Righter, K., Pando, K. M., Danielson, L., & Lee, C. T. (2010). Partitioning of Mo, P and other siderophile elements (Cu, Ga, Sn, Ni, Co, Cr, Mn, V, and W) between metal and silicate melt as a function of temperature and silicate melt composition. *Earth and Planetary Science Letters*, *291*(1–4), 1–9. <https://doi.org/10.1016/j.epsl.2009.12.018>
- Ruiz, D., Ros-Yanez, T., Ortega, L., Sastre, L., Vandenbossche, L., Legendre, B., et al. (2005). Effect of atomic order on the electrical and magnetic properties of Fe_{100-x}Si_x (6 < x < 14) alloys. *IEEE Transactions on Magnetics*, *41*(10), 3286–3288. <https://doi.org/10.1109/TMAG.2005.854723>
- Scheinberg, A., Soderlund, K. M., & Schubert, G. (2015). Magnetic field generation in the lunar core: The role of inner core growth. *Icarus*, *254*, 62–71. <https://doi.org/10.1016/j.icarus.2015.03.013>
- Scott, H., Kiefer, B., Martin, C. D., Boateng, N., Frank, M., & Meng, Y. (2008). P–V equation of state for Fe₂P and pressure-induced phase transition in Fe₂P. *High Pressure Research*, *28*(3), 375–384. <https://doi.org/10.1080/08957950802246506>
- Scott, H. P., Huggins, S., Frank, M. R., Maglio, S. J., Martin, C. D., Meng, Y., et al. (2007). Equation of state and high-pressure stability of Fe₃P-schreibersite: Implications for phosphorus storage in planetary cores. *Geophysical Research Letters*, *34*, L06302. <https://doi.org/10.1029/2006GL029160>
- Seagle, C. T., Cottrell, E., Fei, Y., Hummer, D. R., & Prakapenka, V. B. (2013). Electrical and thermal transport properties of iron and iron–silicon alloy at high pressure. *Geophysical Research Letters*, *40*, 5377–5381. <https://doi.org/10.1002/2013GL057930>
- Secco, R. A. (2017). Thermal conductivity and Seebeck coefficient of Fe and Fe–Si alloys: Implications for variable Lorenz number. *Physics of the Earth and Planetary Interiors*, *265*, 23–34. <https://doi.org/10.1016/j.pepi.2017.01.005>
- Secco, R. A., & Schloessin, H. H. (1989). The electrical resistivity of solid and liquid Fe at pressures up to 7 GPa. *Journal of Geophysical Research*, *94*(B5), 5887. <https://doi.org/10.1029/JB094iB05p05887>
- Sha, L. (2000). Whitlockite solubility in silica melts: some insights into lunar and planetary evolution. *Geochimica et Cosmochimica Acta*, *64*(18), 3217–3236. [https://doi.org/10.1016/S0016-7037\(00\)00420-8](https://doi.org/10.1016/S0016-7037(00)00420-8)
- Silber, R. E., Secco, R. A., & Yong, W. (2017). Constant electrical resistivity of Ni along the melting boundary up to 9 GPa. *Journal of Geophysical Research: Solid Earth*, *122*, 5064–5081. <https://doi.org/10.1002/2017JB014259>
- Silber, R. E., Secco, R. A., Yong, W., & Littleton, J. A. H. (2018). Electrical resistivity of liquid Fe to 12 GPa: Implications for heat flow in cores of terrestrial bodies. *Scientific Reports*, *8*(1), 10,758–10,759. <https://doi.org/10.1038/s41598-018-28921-w>
- Spohn, T., Konrad, W., Breuer, D., & Ziethe, R. (2001). The longevity of lunar volcanism: implications of thermal evolution calculations with 2D and 3D mantle convection models. *Icarus*, *149*(1), 54–65. <https://doi.org/10.1006/icar.2000.6514>
- Steenstra, E. S., Lin, Y., Rai, N., Jansen, M., & van Westrenen, W. (2017). Carbon as the dominant light element in the lunar core. *American Mineralogist*, *102*(1), 92–97. <https://doi.org/10.2138/am-2017-5727>

- Steenstra, E. S., Rai, N., Knibbe, J. S., Lin, Y., & van Westrenen, W. (2016). New geochemical models of core formation in the Moon from metal-silicate partitioning of 15 siderophile elements. *Earth and Planetary Science Letters*, *441*, 1–9. <https://doi.org/10.1016/j.epsl.2016.02.028>
- Stewart, A. J., & Schmidt, M. W. (2007). Sulfur and phosphorus in the Earth's core: The Fe-P-S system at 23 GPa. *Geophysical Research Letters*, *34*, L12201. <https://doi.org/10.1029/2007GL030138>
- Suehiro, S., Ohta, K., Hirose, K., Morard, G., & Ohishi, Y. (2017). The influence of sulfur on the electrical resistivity of hcp iron: Implications for the core conductivity of Mars and Earth. *Geophysical Research Letters*, *44*, 8254–8259. <https://doi.org/10.1002/2017GL074021>
- Sundqvist, B. (1988). Electrical resistance of nickel in the range 300–725 K and 0–2 GPa. *Physical Review B*, *38*(17), 12,283–12,289. <https://doi.org/10.1103/PhysRevB.38.12283>
- van der Pauw, L. J. (1958). A method of measuring specific resistivity and Hall effect of discs of arbitrary shape. *Philips Research Reports*, *13*(1), 1–9.
- Varga, L. K., Mazaleyrat, F., Kovac, J., & Greneche, J. M. (2002). Structural and magnetic properties of metastable Fe_{1-x}Si_x (0.15 < x < 0.34) alloys prepared by a rapid-quenching technique. *Journal of Physics: Condensed Matter*, *14*(8), 1985–2000. <https://doi.org/10.1088/0953-8984/14/8/326>
- Wagle, F., & Steinle-Neumann, G. (2018). Electrical resistivity discontinuity of iron along the melting curve. *Geophysical Journal International*, *213*(1), 237–243. <https://doi.org/10.1093/gji/ggx526>
- Wagle, F., Steinle-Neumann, G., & de Koker, N. (2018). Resistivity saturation in liquid iron–light-element alloys at conditions of planetary cores from first principles computations. *Comptes Rendus Geoscience*, *351*(2-3), 154–162. <https://doi.org/10.1016/j.crte.2018.05.002>
- Weber, R. C., Lin, P. Y., Garnero, E. J., Williams, Q., & Lognonné, P. (2011). Seismic detection of the lunar core. *Science*, *331*(6015), 309–312. <https://doi.org/10.1126/science.1199375>
- Wegliński, B., & Kaczmar, J. (1980). Effect of Fe₃P addition on magnetic properties and structure of sintered iron. *Powder Metallurgy*, *23*(4), 210–216. <https://doi.org/10.1179/pom.1980.23.4.210>
- Westerstrandh, B., Lundgren, L., Gäfvert, U., & Carlsson, B. (1977). Magnetic susceptibility resistivity and thermal expansion measurements on FeP. *Physica Scripta*, *15*(4), 276–280. <https://doi.org/10.1088/0031-8949/15/4/009>
- Wieczorek, M. A. (2006). The constitution and structure of the lunar interior. *Reviews in Mineralogy and Geochemistry*, *60*(1), 221–364. <https://doi.org/10.2138/rmg.2006.60.3>
- Williams, J. G., Boggs, D. H., Yoder, C. F., Ratcliff, J. T., & Dickey, J. O. (2001). Lunar rotational dissipation in solid body and molten core. *Journal of Geophysical Research*, *106*(E11), 27,933–27,968. <https://doi.org/10.1029/2000JE001396>
- Williams, J. G., Konopliv, A. S., Boggs, D. H., Park, R. S., Yuan, D. N., Lemoine, F. G., et al. (2014). Lunar interior properties from the GRAIL mission. *Journal of Geophysical Research: Planets*, *119*, 1546–1578. <https://doi.org/10.1002/2013JE004559>
- Wood, B. J., Walter, M. J., & Wade, J. (2006). Accretion of the Earth and segregation of its core. *Nature*, *441*(7095), 825–833. <https://doi.org/10.1038/nature04763>
- Wu, X., Mookherjee, M., Gu, T., & Qin, S. (2011). Elasticity and anisotropy of iron-nickel phosphides at high pressures. *Geophysical Research Letters*, *38*, L20301. <https://doi.org/10.1029/2011GL049158>
- Wu, X., & Qin, S. (2010). First-principles calculations of the structural stability of Fe₂P. *Journal of Physics: Conference Series*, *215*, 012110. <https://doi.org/10.1088/1742-6596/215/1/012110>
- Yan, H. (2015). Pressure-induced structural phase transition in iron phosphide. *Computational Materials Science*, *107*, 204–209. <https://doi.org/10.1016/j.commatsci.2015.05.031>
- Yin, Y., Li, Z., & Zhai, S. (2019). The phase diagram of the Fe-P binary system at 3 GPa and implications for phosphorus in the lunar core. *Geochimica et Cosmochimica Acta*, *254*, 54–66. <https://doi.org/10.1016/j.gca.2019.03.037>
- Yousuf, M., Sahu, P. C., & Rajan, K. G. (1986). High-pressure and high-temperature electrical resistivity of ferromagnetic transition metals: Nickel and iron. *Physical Review B*, *34*(11), 8086–8100. <https://doi.org/10.1103/PhysRevB.34.8086>
- Zaitsev, A. I., Dobrokhotova, Z. V., Litvina, A. D., & Mogutnov, B. M. (1995). Thermodynamic properties and phase equilibria in the Fe-P system. *Journal of the Chemical Society, Faraday Transactions*, *91*(4), 703–712. <https://doi.org/10.1039/FT9959100703>
- Zhang, C., Lin, J., Liu, Y., Feng, S., Jin, C., Hou, M., & Yoshino, T. (2018). Electrical resistivity of Fe-C alloy at high pressure: effects of carbon as a light element on the thermal conductivity of the Earth's core. *Journal of Geophysical Research: Solid Earth*, *123*, 3564–3577. <https://doi.org/10.1029/2017JB015260>
- Zhang, N., Parmentier, E. M., & Liang, Y. (2013). A 3-D numerical study of the thermal evolution of the Moon after cumulate mantle overturn: The importance of rheology and core solidification. *Journal of Geophysical Research: Planets*, *118*, 1789–1804. <https://doi.org/10.1002/jgre.20121>
- Zhao, Z., Liu, L., Zhang, S., Yu, T., Li, F., & Yang, G. (2017). Phase diagram, stability and electronic properties of an Fe–P system under high pressure: A first principles study. *RSC Advances*, *7*(26), 15,986–15,991. <https://doi.org/10.1039/C7RA01567D>
- Ziethe, R., Seiferlin, K., & Hiesinger, H. (2009). Duration and extent of lunar volcanism: Comparison of 3D convection models to mare basalt ages. *Planetary and Space Science*, *57*(7), 784–796. <https://doi.org/10.1016/j.pss.2009.02.002>
- Zuber, M. T., Smith, D. E., Asmar, S. W., Konopliv, A. S., Lemoine, F. G., Melosh, H. J., et al. (2011). Mission status and future prospects for improving understanding of the internal structure and thermal evolution of the Moon from the gravity recovery and interior laboratory (GRAIL) mission. *Lunar and Planetary Science Conference*, *42*, 1967.